

Vortices in the wakes of AGB stars

C. J. Wareing¹, Albert A. Zijlstra¹ and T. J. O'Brien²

ABSTRACT

Vortices have been postulated at a range of size scales in the universe including at the stellar size-scale. Whilst hydrodynamically simulating the wind from an asymptotic giant branch (AGB) star moving through and sweeping up its surrounding interstellar medium (ISM), we have found vortices on the size scale of 10^{-1} pc to 10^1 pc in the wake of the star. These vortices appear to be the result of instabilities at the head of the bow shock formed upstream of the AGB star. The instabilities peel off downstream and form vortices in the tail of AGB material behind the bow shock, mixing with the surrounding ISM. We suggest such structures are visible in the planetary nebula Sh 2-188.

Subject headings: hydrodynamics – turbulence – stars: AGB and post-AGB – circumstellar matter – ISM: structure – stars: mass-loss

1. Introduction

Vortex instabilities are observed throughout the universe. On the smallest scales in the laboratory, Robey et al. (2002) have experimentally investigated the 3D interaction of a strong shock with a spherical density inhomogeneity via laser-driven experiments. They found a double vortex ring structure and an azimuthal instability that ultimately results in the breakup of the ring. They also performed 3D computational simulations which were shown to be in remarkable agreement with their experimental investigations.

In planetary atmospheres, vortices can be regularly observed in von Karman vortex streets often associated with atmospheric flow past stationary objects such as mountains. They have also been suggested as the explanation of the giant storm on Jupiter known as the Great Red Spot (Williams 1997). Atmospheric simulations have successfully reproduced

¹School of Physics and Astronomy, University of Manchester, Campus North, PO Box 88, Manchester, M60 1QD, UK; c.j.wareing@manchester.ac.uk, a.zijlstra@manchester.ac.uk

²Jodrell Bank Observatory, University of Manchester, Macclesfield, SK11 9DL, UK; tim.obrien@manchester.ac.uk

vortices comparable to the Great Red Spot (Yamazaki et al. 2004) and other vortex anomalies in the atmosphere of Jupiter (Morales-Juberias & Dowling 2005). Li et al. (2001) have hydrodynamically simulated vortices at the stellar size scale in thin accretion disks.

Vortices at the interstellar size scale have been predicted since some of the first 'high' resolution calculations by Woodward (1976) where Kelvin-Helmholtz instabilities begin the breakup of interstellar clouds. More recently, Klein et al. (1994) predicted the existence of such vortices forming from the interaction of strong shocks with the medium through which they propagate. A series of laboratory experiments as well as two- and three-dimensional simulations (Klein et al. 2003) confirmed these earlier predictions. They modelled the interaction of a supernova shock and a cloud in the interstellar medium (ISM) as the effect of a high density sphere embedded in a low density medium after the passage of a strong shock wave. They found vortex rings are shed from the sphere and, importantly, these vortex rings break up at high Mach number due to three-dimensional bending-mode vortex-ring instabilities. Since their simulations are isothermal, they can be scaled to any size, for the given Mach number, and so are relevant to clouds in the ISM ranging from the smallest resolved structures at $\sim 10^{-3}$ pc to diffuse clouds up to 100 pc.

Vortices can act as a source of local angular momentum and turbulence, both of which are important in the evolution of molecular clouds. For a discussion of the importance of interstellar turbulence, we refer to the two-part review by Elmegreen & Scalo (2004a,b). Such molecular clouds are themselves important for star formation (Tilley & Pudritz 2004). Vortices in the ISM can also affect anything expanding into this medium e.g. supernovae, novae and planetary nebulae.

In this paper, we present simulations that show under certain conditions von Karman-like vortices are produced in the wakes of asymptotic giant branch (AGB) stars with size scales from 10^{-1} pc to 10^1 pc. Specifically, we model the interaction of a stellar wind with the ISM where the star has a significant motion through the ISM. The stellar wind in our simulation is produced by an AGB star (Wareing et al. 2006b). AGB stellar winds have typical speeds of $\sim 15 \text{ km s}^{-1}$ and mass-loss rates $\dot{M} \sim 10^{-7}\text{--}10^{-5} \text{ M}_\odot \text{ yr}^{-1}$. This wind ejects up to a few solar masses of material into the surrounding medium over the course of $\sim 500\,000$ years. In our two-wind model, we have found that the movement of the star through the ISM (modelling the ISM as a second wind) causes the ejected stellar material to form into a bow shock upstream of the star with a tail flowing downstream. It is in this tail that we find evidence of von Karman-like vortices. Observational evidence for interaction between the ISM and AGB winds has been found by Zijlstra & Weinberger (2002) and Schöeier et al. (2005) and a model of the interaction has been used to explain the shape of the structure around R Hya as a bow shock (Ueta et al. 2006; Wareing et al. 2006b).

In hindsight, previous 2D astrophysical simulations considering this phase of stellar evolution have produced such vortices (see figure 18 of Szentgyorgyi et al. 2003), but the authors did not discuss them. We consider the vortices in 3D allowing an investigation and description of their behaviour.

2. Simulations

A computational fluid dynamics (CFD) scheme, CUBEMPI, has been used to hydrodynamically simulate the interaction of a star moving through the ISM ejecting a stellar wind during the AGB phase of evolution. The numerical scheme is based on a second-order Godunov scheme due to Falle (1991). The Riemann solver is due to van Leer (1979). The scheme is Eulerian, posed in three dimensions and cartesian coordinates and is fully parallel using the MPI¹ library of subroutines. The scheme also includes the effect of radiative cooling via a parametric fit to the cooling curve of Raymond et al. (1976) above 10^4 K. The scheme has been fully tested using standard CFD tests and its performance in these tests compared to results obtained by Liska & Wendroff (2003) for other CFD schemes. Astrophysical tests have also been performed using the Sedov and Primakoff analytical supernova models. The full details of the scheme and its performance can be found in Wareing (2005).

We have used a two-wind model with a numerical domain of 200^3 cells. This model is the same as that used to successfully model the structure around R Hya (Wareing et al. 2006b). It is also the AGB stage of our triple-wind model following the AGB and post-AGB phases of evolution used to successfully model the planetary nebula (PN) Sh 2-188 (Wareing et al. 2006a). We have considered four values of the mass-loss rate on the AGB: 10^{-7} , 5×10^{-7} , 10^{-6} & 5×10^{-6} $M_\odot \text{ yr}^{-1}$. We have considered the AGB phase, and hence the simulation, to last 500 000 years with an AGB wind velocity of 15 km s^{-1} . These wind parameters are typical of previous models in the literature (Mellema et al. 1991; Frank & Mellema 1994). An unphysical temperature of 10^4 K was used for the AGB wind but this does not affect the overall result (Wareing et al. 2006b). In view of the still considerable uncertainties on the detailed properties and evolution of these winds, more detailed temporal variations were not modelled. Relative velocities of the star with respect to the ISM have been considered from 0 to 200 km s^{-1} in steps of 25 km s^{-1} corresponding to the range of velocities found within the Galaxy. With speeds of relative movement above 75 km s^{-1} , we have not simulated mass-loss rates of $10^{-7} M_\odot \text{ yr}^{-1}$ due to CPU constraints. The ISM has been modelled with densities $n_H = 2$, 0.1 & 0.01 cm^{-3} and a temperature of 8×10^3 K. These are the

¹<http://www-unix.mcs.anl.gov/mpi/>

properties of the warm ISM or WIM, the larger constituent of the ISM (Burton 1988).

The simulations begin at the start of the AGB phase of evolution of the central star and are performed in the frame of reference of the star. The wind from the star drives a shock into the ISM. In the case of a stationary star we have found the shock drives a spherical shell of AGB wind material sweeping up ISM material. Inside the reverse shock is a bubble of undisturbed AGB wind material. This bubble is of low density and temperature, increasing towards the star, and of high pressure. If the central star is moving through the ISM, a bow shock forms upstream of the star. Such bow shocks have been simulated in other cases of winds interacting with injected flows (Villaver, Garcia-Segura & Manchado 2003; Pittard et al. 2005). Eventually, the simulations show the bow shock reaches a maximum distance ahead of star which can be understood in terms of a ram pressure balance between the stellar wind and the ISM. Strong shock theory predicts the temperature of the shocked material at the head of the bow shock: $T \sim 3/16 m v^2/k$ in general agreement with the simulations. Ram-pressure-stripped material from the head of the bow shock forms a tail behind the nebula. As material moves down the tail, it cools and mixes with ISM material.

3. Results

Figure 1 shows two snapshots from the AGB evolution of a central star moving at 75 km s^{-1} . Both panels show the gas state at the end of the AGB phase, 500 000 years into the simulation. In the left panel, the bow shock driven by the AGB wind has reached a stationary position at the point of ram pressure balance, 0.02 pc ahead of the central star, with a smooth tail of shocked material extending downstream of the bow shock. In the right panel, where the mass-loss rate is 50 times higher, the tail contains vortices flowing downstream.

Figure 2 shows the evolution of the vortex in the right panel of Figure 1. In the top panel, the indentation near the head of bow shock indicates an instability, which in the second panel is shed downstream from the head of the bow shock. The remaining panels show the instability forming into a vortex, spiralling and flowing downstream. This episode of vortex shedding from the head of the bow shock is not the first such event. After 50 000 years of evolution, the tail appears to become turbulent and the first episode of vortex shedding begins at 90 000 years. The initial episode appears to be symmetric around the bow shock and the instability forms into a vortex ring flowing downstream. The next episode begins at 205 000 years and continues with multiple episodes of vortex shedding with no clear periodicity or ring symmetry. The vortices flow out of the simulation domain in 100 000 years having achieved a stable structure which suggests they will have an extended lifetime in the

wake.

To show the breakdown of the later vortices azimuthally, Figure 3 shows a visualisation of the density datacube 500 000 years into the simulation. An azimuthally-unstable partial vortex ring can be seen mid-way down the tail and more partial vortex-rings are in the process of shedding off the bow shock.

In order to investigate the effect of grid resolution on the production of vortices, the same simulation which produces vortices with a movement through the ISM of 75 km s^{-1} was rerun at a grid resolution of 100^3 and 300^3 . The low resolution simulation showed a smooth, steady state tail with no clear vortices produced from the head of the bow shock. Undulations at the head of the bow shock do appear to move down the tails. We suggest the initial instabilities which lead to vortices downstream are strongly suppressed by this low resolution. At 300^3 , many more vortices than at 200^3 seem to be produced from similar instabilities at the head of the bow shock, but importantly the physical size of the vortices is similar and therefore not dependent on resolution. A 2D numerical simulation was also performed in cylindrical polar coordinates for further comparison. Similar vortex-like structures form in the tail of AGB material and flow downstream. The initial instability appears to be slower in developing and once developed, the instability causes a periodic movement of the tails more like von Karman vortices. The vortices themselves appear as density enhancements moving down the tail structure. Clearly in 3D simulations the vortices form fully and the periodicity is destroyed by the instability of the bow shock following the launching of the first vortex ring.

4. Discussion

We postulate that the vortices in the tail are the result of vortex shedding from the head of the bow shock. Vortex shedding occurs when a fluid passes by an object and the shear layer near the object creates a velocity gradient. The Kelvin-Helmholtz instability often accompanies flows where shear is present, making the flow unstable to perturbations. The simulations show that the bow shock does not remain stationary in the frame of reference of the star after it has reached the ram pressure balance point. In fact, its distance ahead of the star is oscillating and it is the Kelvin-Helmholtz instability which is responsible for this oscillation. As the instabilities spread from the head of the bow shock, peel off and flow downstream to form vortices, the bow shock loses material in the vortices and is driven back towards the star by the pressure of the ISM. As the stellar wind supplies more material to the bow shock, it recovers its ram-pressure-balance position and this instability-driven oscillation begins again. Note that this shows that instabilities set in only after the bow shock has reached its balance position, and thus vortices only appear in the tail after this

time.

Figure 4 shows the PN Sh 2-188 in the left panel and a detail of the nebula in the right panel. In a previous paper, Wareing et al. (2006a) modelled Sh 2-188 as a nebula shaped by wind-ISM interaction where the bright arc is a bow shock ahead of the central star. The structures highlighted in the right panel can be interpreted in our vortex-shedding scenario as instabilities being peeled off the bow-shock which will form vortices downstream.

Theoretically, vortices form over a certain range of Reynolds number. The Reynolds number of a flow is defined as the ratio of internal forces to viscous forces and can be formulated as $Re = \rho V D/\nu$ where ρ is the fluid density, V is the free-stream fluid velocity, D is the characteristic length and ν is the dynamic fluid viscosity. For a Reynolds number of less than 50, the wake behind an object is thin and the flow can be classed as laminar. With a Reynolds number around 100, features similar to the von Karman vortex street develop as we see here. The wake also can become several times wider than the characteristic width of the object. At Reynolds numbers of 1000 and greater, the wake behind the object becomes turbulent. It is difficult to estimate the Reynolds numbers in our simulations as this involves the viscosity of the fluid and the simulations include an artificial viscosity to suppress the Quirk instability (Quirk 1994). Since this artificial viscosity is constant in all the simulations, it is possible to estimate *relative* Reynolds numbers between the simulations. The characteristic length in a particular simulation is estimated as the diameter of the object in the flow, defined by twice the ram-pressure-balance distance. Note that the point of ram pressure balance is inversely proportional to flow-velocity and thus so is the characteristic length. Therefore, there is no dependency on flow-velocity in the estimation of relative Reynolds numbers. The relative Reynolds number increases with increasing mass-loss rate and increasing ISM density. In the simulations, there is a general trend to see vortices when the mass-loss rates or ISM densities are not extreme. These simulations correspond to the mid-range of relative Reynolds numbers. However, in some cases of extreme mass-loss rate or ISM density, the bow shock structure is either so large that it is possible we do not see vortices on the simulation timescale, or so small that it is possible the ISM flow confines the bow shock enough to suppress the formation of vortices. Thus, it is not clear whether the vortices are dependent on relative Reynolds number although it seems there is a range where vortices are more apparent on the timescales of these AGB simulations, which we might expect from theoretical indications. All the simulations are supersonic from a Mach number of 1.8 at 25 km s^{-1} to 14.4 at 200 km s^{-1} suggesting no dependency on Mach number.

The vortex shedding lacks the regular period seen in the case of von Karman vortices. We do note though that the first episode of vortex shedding is in the form of a symmetric ring shed downstream from the head of the bow shock. Further episodes of vortex shedding

do not shed such stable rings and vortices are shed from either side of the bow shock. This can be understood in terms of the regular shape of the bow shock at the time of the first vortex shedding instability; following this, vortex shedding occurs from an irregular bow shock and results in irregular behaviour.

AGB winds are important sources of dust and light elements and thus for the evolution of the global ISM, but their importance to the dynamics of the ISM has not previously been considered. Our results show that several vortices can be launched into the ISM during the AGB phase of evolution. These improve the mixing of material, and provide the local ISM with a source of angular momentum. Our simulations suggest the vortices are long-lived since they appear to form stable structures which flow out of the simulation domain.

The space density of mass-losing AGB stars is low ($\sim 100 \text{ kpc}^{-3}$), and assuming a typical life time of the phase of 10^5 yrs, each region in the ISM may be affected by the tail of an AGB star every 10^9 yrs. We estimate the power input into the ISM from AGB winds to be $2.5 - 125 \times 10^{-32} \text{ erg cm}^{-3} \text{ s}^{-1}$. This is several orders of magnitude less than the contribution of supernovae and winds from massive stars at around $10^{-25} \text{ erg cm}^{-3} \text{ s}^{-1}$ (Elmegreen & Scalo 2004). We find the temperature of material in the vortices to be on the order of 5-10 000 K, cooling as the vortex moves downstream. The global (as opposed to the local) importance of the vortices may therefore be limited and possibly the angular momentum returned to the local ISM may be most important. It is also possible that the galactic distribution of AGB stars provides a source of turbulence where supernovae and winds from massive stars do not. One may also expect similar vortices to form behind other types of mass-losing stars. We suggest that the swirls seen in the light echo of V838 Mon (Bond 2006) could represent such vortices.

In our simulations we have modelled the ISM with a constant density. In reality, the ISM is unlikely to be homogeneous and this will more than likely affect the structures forming around the star. It is possible that inhomogeneities would fracture the bow shock, as seen in the case of the PN Sh 2-188 (Wareing et al. 2006a), and seed more vortex shedding. Further, a star travelling at 200 km s^{-1} would travel approximately 100 pc during the AGB phase and with a bow shock cross-section of up to $\sim 2.0 \text{ pc}^2$, interact with a volume of ISM of up to 200 pc^3 , which could contain on the order of a few tens of stars which could interact with the vortices.

In our simulations, we have neglected viscosity and observed a variety of behaviour from low to high relative Reynolds numbers. Magnetic fields may suppress viscosity significantly implying a greater degree of turbulence. However, large amounts of viscosity in the ISM would smooth the structures which develop in our simulations. It is for this reason that it would be premature to quantify when to expect vortices for particular stellar parameters.

The authors acknowledge very useful comments from the anonymous referee and Professor John Scalo. CJW acknowledges the support of PPARC. The numerical computations were carried out using the COBRA supercomputer at Jodrell Bank Observatory.

REFERENCES

Binney, J., & Merrifield, M. 1998, Galactic Astronomy (Princeton, NJ: Princeton University Press), Ch. 10

Bond, H. 2006, preprint(astro-ph/0608222)

Burton, W. B. 1988, Galactic and Extragalactic Radio Astronomy (New York: Springer), 295

Drew, J. E., et al., 2005, MNRAS, 362, 753

Elmegreen, B. G., & Scalo, J. 2004, ARA&A, 42, 211

Elmegreen, B. G., & Scalo, J. 2004, ARA&A, 42, 275

Falle, S. A. E. G. 1991, MNRAS, 250, 581

Frank, A., & Mellema, G. 1994, ApJ, 430, 800

Klein, R. I., McKee, C. F., Colella, P. 1994, ApJ, 420, 213

Klein, R. I., Budil, K. S., Perry, T. S., Bach, D. R. 2003, ApJ, 583, 245

Li, H., Colgate, S. A., Wendroff, B., Liska, R. 2001, ApJ, 551, 874

Liska, R., & Wendroff, B. 2003, SIAM J. Sci. Comput., 25, 995

van Leer, B. 1979, J. Chem. Phys., 32, 101

Mauron, N., & Huggins, P. J. 2006, A&A, 452, 257

Mellema, G., Eulderink, F., & Icke, V. 1991, A&A, 252, 718

Morales-Juberias, R., & Dowling T. E., 2005, P&SS, 53, 1221-1233

Pittard, J. M., et al., 2005, MNRAS, 361, 1077

Quirk, J. J. 1994, Int. J. Numer. Meth. Fl., 18, 555

Raymond, J. C., Cox, D. P., & Smith, B. W. 1976, *ApJ*, 204, 290

Robey, H. F., et al., 2002, *Phys. Rev. Lett.*, 89, 085001

Schöier, F. L., Lindqvist, M., & Olofsson, H. 2005, *A&A*, 436, 633

Szentgyorgyi, A., Raymond, J., Franco, F., Villaver, E. & Lopez-Martin, L. 2003, *ApJ*, 594, 874

Tilley, D. A., & Pudritz, R. E. 2004, *MNRAS*, 353, 769

Ueta, T., et al. 2006, *ApJ*, 648, L39

Villaver, E., Garcia-Segura, G., Manchado, A., 2003, *ApJL*, 585, L49

Wareing, C. J. 2005, PhD thesis, Univ. of Manchester

Wareing, C. J., et al., 2006a, *MNRAS*, 366, 387

Wareing, C. J., et al., 2006b, *MNRAS*, 372, L63

Williams, G. P. 1997, *JGR*, 102, 9303

Woodward, P. R. 1976, *ApJ*, 207, 484

Yamazaki, Y. H., Skeet, D. R., & Read, P. L. 2004, *P&SS*, 52, 423-445

Zijlstra, A. A., & Weinberger, R. 2002, *ApJ*, 572, 1006

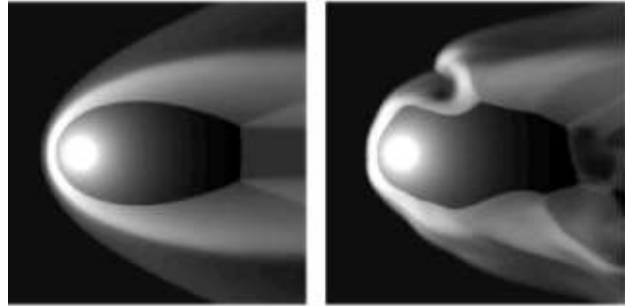


Fig. 1.— Snapshots of the logarithm of density from simulations of the AGB evolution of a central star moving at 75 km s^{-1} . The ISM is flowing from left to right. Both simulations have an ISM density $n_{\text{H}} = 2 \text{ cm}^{-3}$. The left panel has a mass-loss rate of $10^{-7} \text{ M}_{\odot} \text{ yr}^{-1}$ and is 0.25 pc on a side. The right panel has a mass-loss rate of $5 \times 10^{-6} \text{ M}_{\odot} \text{ yr}^{-1}$ and is 1.75 pc on a side.

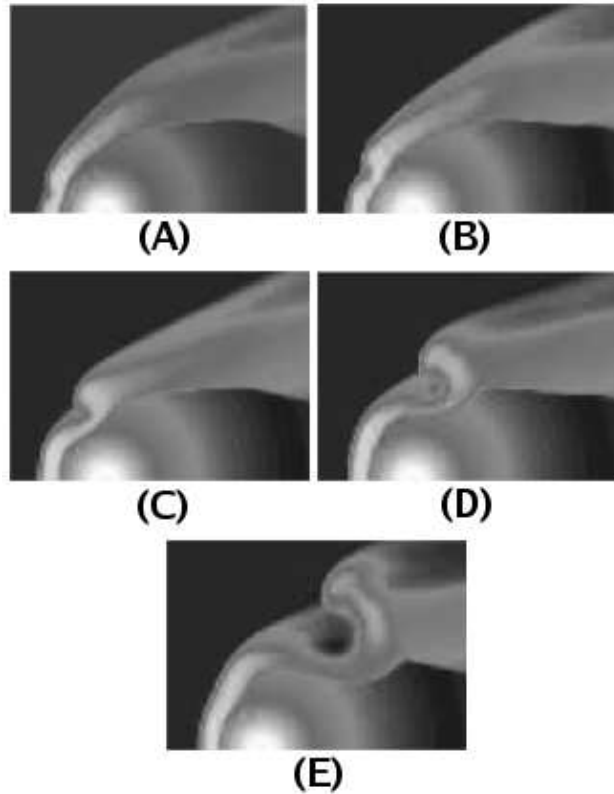


Fig. 2.—Shedding of the vortex in detail. The panels show portions of slices of the logarithm of density through the position of the central star parallel to the direction of motion. Panel A is at 460 000 years into the AGB phase, panel B 470 000 years, panel C 480 000 years, panel D 490 000 years and panel E 500 000 years.

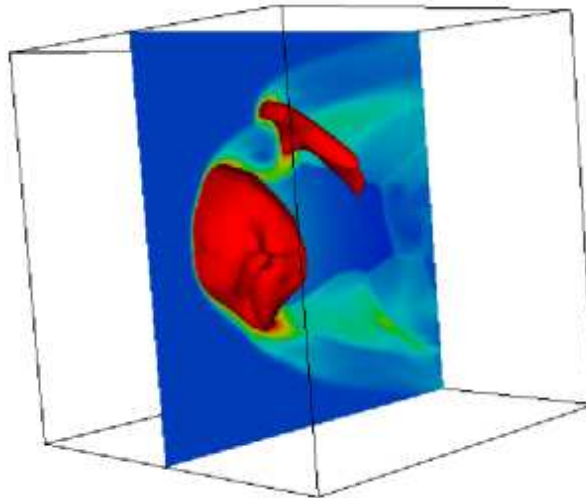


Fig. 3.— Visualisation of the simulation datacube showing gas density using the visualisation software package MAYAVI at the same time as Figure 1. A planar slice through the position of the central star and parallel to the direction of motion is shown. This slice is intersected by a 3D isosurface of constant density (in red) demonstrating the shape of the bow shock with a vortex arc further downstream. Note that the vortex downstream has become azimuthally unstable.

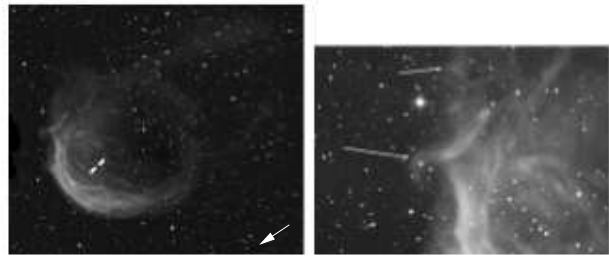


Fig. 4.— $\text{H}\alpha$ images showing the PN Sh 2-188. On the left is a combined image of the whole nebula showing the bright south-eastern arc and the faint north-western structures interpreted as a bow shock and tail respectively. The nebula is 11 arcminutes in diameter with a tail of 18 arcminutes. In the left panel, the central star is indicated between the markers, with the arrow indicating its proper motion. For more information, refer to Wareing et al. (2006a). We interpret the structures indicated by arrows in the right panel as instabilities being shed from the bow-shock. The images are mosaics taken as part of the Isaac Newton Telescope Photometric $\text{H}\alpha$ Survey of the Northern Galactic Plane (IPHAS) (Drew et al. 2005) in 2003. North is up and East is to the left. The left image is 20×16.7 arcmin. and the right image is 7.6×5.3 arcmin.